EBioMedicine 37 (2018) 246–258

Contents lists available at ScienceDirect

EBioMedicine

journal homepage: www.ebiomedicine.com

EBioMedicine
Published by THE LANCET

Salvianolic acid A targeting the transgelin-actin complex to enhance vasoconstriction

Weilong Zhong [a,b,1], Bo Sun [b,1], Wenqing Gao [c,1], Yuan Qin [a,b,1], Heng Zhang [a,b,1], Longcong Huai [a], Yuanhao Tang [a], Yuan Liang [a], Lingfei He [a], Xiaoyun Zhang [a], Honglian Tao [a], Shuang Chen [b], Wei Yang [b], Lan Yang [b], Yanrong Liu [b], Huijuan Liu [a,b], Honggang Zhou [a,b,*], Tao Sun [a,b,*], Cheng Yang [a,b,*]

[a] State Key Laboratory of Medicinal Chemical Biology and College of Pharmacy, Nankai University, Tianjin 300000, China
[b] Tianjin Key Laboratory of Molecular Drug Research, Tianjin International Joint Academy of Biomedicine, Tianjin 300000, China
[c] Heart Center, Tianjin Third Central Hospital, Tianjin 300170, China

ARTICLE INFO

Article history:
Received 11 August 2018
Received in revised form 13 October 2018
Accepted 13 October 2018
Available online 23 October 2018

Keywords:
Transgelin
Actin
SAA
Vascular smooth muscle cell
Myocardial ischemia

ABSTRACT

Background: Salvia miltiorrhiza is used extensively to treat cardiovascular diseases. SAA is a major bioactive component in *Salvia miltiorrhiza* and mediates myocardial ischemia (MI). However, the industrial production of SAA is limited due to low yields. In addition, the direct targets of SAA are unknown. Here we explore cardioprotective mechanisms and targets of SAA in the cardiovascular system.

Methods: Transgelin and actin were identified as targets of SAA using a chemical biology method and were validated by Biacore analysis, microscale thermophoresis and single-molecule imaging. Studies of transgelin (−/−) knockout mice further verify the target. Cardioprotective mechanisms and targets of SAA were studied in cultured vascular smooth muscle cells and transgenic mice.

Findings: In WT mice, SAA targeted transgelin and had a protective effect on myocardium but did not have the same protective effect on transgelin (−/−) mice. SAA stabilizes the transgelin-actin complex, modulates the reorganization of the actin cytoskeleton, facilitates F-actin bundling, further enhances the contractility and blood flows of coronary arteries, and improves outcomes of myocardial ischemia. Based on the target, a more active SAA derivative offering myocardial protection, SAA-30, was obtained.

Interpretation: We report on the direct targets of SAA and mechanisms of myocardial ischemia treatment. We also find that transgelin may act as a novel therapeutic target of myocardial ischemia. Furthermore, a more effective derivative of SAA provides the basis for further clinical translational research.

Abbreviations

SAA	salvianolic acid A
MI	myocardial ischemia
SAB	salvianolic acid B
HVSMC	human vascular smooth muscle cell
CASMC	Coronary Artery Smooth Muscle Cell
MST	microscale thermophoresis
STORM	stochastic optical reconstruction microscopy
WT	wild type
CK	creatine kinase
CK-MB	creatinine kinase MB isoenzyme
AST	aspartate transaminase
LDH	lactate dehydrogenase

1. Introduction

Myocardial ischemia involves a lack of coronary blood flow for the myocardium. Increasing effective blood supplies available to myocardial tissue can improve myocardial ischemia outcomes. *Danshen*, a well-known Chinese medical material, has long been used to promote blood flow and to resolve blood stasis with considerable efficacy [1–3]. SAA and salvianolic acid B (SAB) are the two main water-soluble compounds found in *Danshen*. SAA is present at low concentrations in

* Corresponding authors at: State Key Laboratory of Medicinal Chemical Biology and College of Pharmacy, Nankai University, Tianjin 300350, China.
E-mail addresses: honggang.zhou@vip.126.com (H. Zhou), sunrockmia@hotmail.com (T. Sun), cheng.yang@nankai.edu.cn (C. Yang).
[1] These authors contributed equally to this work.

https://doi.org/10.1016/j.ebiom.2018.10.041

Research in context

Evidence available prior to this study

Salvianolic acid A (SAA) is a major polyhydroxy compound used in herbal medicine. *Salvia miltiorrhiza* has been shown to affect the treatment of myocardial ischemia. It has been reported that SAA serves as a potent scavenger of ROS during cardiovascular injury and inhibits the adherence of leukocytes to endothelial cells. In addition, SAA inhibits inflammation, regulates the expression of metalloproteinases during cardiovascular injury and maintains coronary arteries and coronary microcirculation.

Added value of this study

Through this study we found that SAA physically bound with transgelin and actin promotes F-actin aggregation and enhances the contractility of vascular smooth muscle cells, thereby ameliorating myocardial ischemia. Transgelin may serve as a potential therapeutic target in the management of myocardial ischemia. In addition, based on the binding mode of SAA and targets, a derivative of SAA, SAA-30, was obtained and was found to be more active than SAA. These results offer mechanistic insights that help explain the bioactivity of SAA for myocardial preservation. SAA-30 is safe to use and may serve as an ideal candidate drug for the prevention and treatment of myocardial ischemia.

Implications of available evidence

Therapeutic targeting of the transgelin/actin complex and the "rope" drug design method developed to modulate vascular smooth muscle contractions is of clinical translational research value for treating myocardial ischemia (MI). Mechanisms of actions of the transgelin/actin complex and of SAA-30 may also contribute to other diseases associated with IR tissue injuries.

Danshen but is more active than SAB [4,5]. The strong clinical effect of SAA relates to its protective role in the cardiovascular system. Although several studies show the protective effects of SAA on the cardiovascular system, direct targets and mechanisms of its role remain elusive [6–9].

Actin and actin-related proteins are the main determinants of cell contractions. Actin cannot provide these functions alone; actin binding proteins (such as transgelin) must regulate the assembly of actin. Transgelin belongs to the family of calponin and its relative molecular mass is 22 kD. Transgelin, a marker gene of differentiated vascular smooth muscle cells, can bind to actin and promote the polymerization of G-actin monomers to F-actin. Transgelin is closely related to the noncalcium-dependent regulation of smooth muscle contraction. Transgelin is involved in the cytoskeletal remodeling of vascular smooth muscle and in the remodeling of extracellular matrixes. Transgelin plays an important role in colorectal cancer, prostate cancer, breast cancer, and lung cancer. Transgelin plays a significant role in several diseases, but there is currently no drug targeted at transgelin. Targeting the transgelin-actin complex may enhance the constricting function of coronary arteries and increase blood flows to the myocardium.

Here we present a new, simple and scalable protocol for the full synthesis of SAA with yields of >21%. We also identify and validate targets of SAA for the cardiovascular system. SAA and its derivatives bind transgelin and actin to regulate stress in smooth muscle cells [10]. Transgelin may be a target for myocardial protective therapy. Targeting transgelin may serve as an effective way of treating myocardial ischemia and myocardial infarctions. Compared to that observed in wild type mice, the myocardial protective effect of SAA is eclipsed in transgelin (−/−) mice [11]. Based on chemical biology assays we designed a more active derivative of SAA, SAA-30, with a rope-like link to transgelin and actin. This work presents molecular mechanisms of SAA involved in the treatment of myocardial ischemia and in developing novel SAA derivatives for the pharmacological treatment of MI.

2. Materials and methods

2.1. Compound characterization

^{1}H and ^{13}C NMR spectra were recorded using a QNP probe at room temperature at 400 MHz and 100 MHz, respectively. NMR spectra were recorded in deuterated chloroform ($CDCl_3$) at room temperature unless otherwise stated. Chemical shifts (δ values) are reported in parts per million and are referenced to the deuterated residual solvent peak. NMR data are reported as δ values (chemical shift, *J*-value (Hz), integration, where s = singlet, d = doublet, t = triplet, q = quartet, and brs = broad singlet). HRESIMS was measured on an Agilent G6224A TOF spectrometer. All reactions were performed in a nitrogen atmosphere in an oven or in flame-dried glassware. Tetrahydrofuran, diethyl ether and dichloromethane were dried before being used. TLC was performed on precoated silica gel GF254 plates (Qingdao Marine Chemical Factory). Column chromatography was performed using silica gel (200–300 mesh, Qingdao Marine Chemical Factory).

2.2. Animal models

All animal procedures were carried out under protocols approved by the Institutional Animal Care and Use Committee. Mice were sacrificed by carbon dioxide asphyxiation. Wild type C57/B16 were purchased from Charles River Laboratories (Beijing, China) and Transgelin knockout (−/−) C57/BL6 mice were purchased from Jackson Laboratories (Bar Harbor, ME, USA). The cre-lox method was used to knock out Transgelin.

For the MI model, 24 randomly selected C57 wild type mice were divided into a normal group, model group, SAA group and SAA-30 group. The normal group and model control group were given normal saline. The SAA and SAA-30 group were given SAA and SAA-30 orally every day, respectively (10 mg/kg). The drug was given once a day for one week. On the fifth day, the MI model group, SAA group and SAA-30 group were given ISO (3 mg/kg), and the normal group was given the same volume of normal saline by intraperitoneal injection. During the experiment, the animals were free to eat and drink. After the seventh day of administration, the rats were anesthetized with 10% chloral hydrate, and electrocardiograms of all mice were obtained by ECG. Twenty four transgenic (−/−) mice were selected, and the experiment was carried out again using the methods described in this section.

2.3. HVSMC and CASMC cultures

HVSMCs were purchased from CHI Scientific, Inc. (Massachusetts, USA) and were stored in DMEM medium containing 10% foetal bovine serum. CASMCs included coronary smooth muscle cells obtained by primary culturing and were stored in DMEM medium containing 10% foetal bovine serum. The cells passed upon confluence at a 1:2 dilution ratio. For experiments, HVSMCs were passed from passage 2 to passage 4.

2.4. Target identification

The SAA-probe was incubated in HVSMCs for 4 h, and the final concentration of the probe was measured as 10 μM. Then, HVSMC cells were harvested and lysed by adding cell lysate (containing 1 mM PMSF) on ice for 30 min, and protein supernatants were collected by centrifugation. Then, click reaction reagents were added and reacted for 2 h. Streptavidin-coated magnetic beads adsorbed SAA-probe binding proteins. The reacted protein solution was added to 1 × loading

buffer. The probe binding proteins were separated using 12% SDS-PAGE. Differential bands were excised and subjected to in-gel digestion followed identification by mass spectrometry (LC-MS/MS).

2.5. Molecular docking

The crystal structure of transgelin and actin was obtained from the Protein Data Bank. The protein structure was prepared by assigning bond orders, by adding hydrogen, by treating disulfides, by optimizing H-bond assignment and by performing energy minimization to relax the structure using the Optimized Potentials for Liquid Simulations (OPLS)-2005 force field in a vacuum. Minimization was terminated when the root-mean-square deviation (RMSD) reached a maximum cutoff of 0.3 Å. The ligand of the crystal structure was used to define the central site of the docking grid box, and xyz dimensions of the docking grid box were set to $60 \times 60 \times 60$. 3D structures of the SAA derivatives were generated with Ligprep and were minimized with force field OPLS-2005.

2.6. Microscale thermophoresis

The fluorescence labeling of transgelin was performed following the protocol for the N-hydroxysuccinimide (NHS) coupling of dye NT647 (NanoTemper Technologies, Munich, Germany) to lysine residues. In brief, 100 μL of a 20 μM solution of transgelin protein in labeling buffer was mixed with 100 μL of 60 μM NT647-NHS fluorophore (NanoTemper Technologies) in labeling buffer and was incubated for 30 min at room temperature (RT). Pretests using premium-coated and standard-treated MST capillaries (NanoTemper Technology) were performed to test for the adsorption of NT647 MEK1 to the capillary walls by analyzing capillary scans recorded by Monolith NT.115 prior to the MST experiments. Interactions observed between salvianolic acid A and NT647-transgelin were established on a Monolith NT.115 instrument (NanoTemper Technologies, Germany) and were used as a positive control during screening. For this purpose, serial dilutions of salvianolic acid A in assay buffer were prepared and mixed 1:1 with a solution of 30–50 nM NT647-transgelin to yield a final volume of 20 μL per dilution. The reaction mixtures were loaded into standard-treated capillaries and then analyzed by MST at 20% and 80% MST power and at a light-emitting diode (LED) intensity of 30%.

2.7. Tension detection of vascular smooth muscle

The experiments were carried out using MP150 with control software AcqKnowledge 4.0. The DA100C amplifier was used for tension signal acquisition, the amplifier was set at 1000, the high pass filter was set at DC, and the low pass filter was set at 10 Hz.

The calibration of the tension transducer prior to its use proved essential. After calibration, the mice were anesthetized with 10% chloral hydrate (normal saline). A segment of the blood vessel was removed, and one end of the blood vessel was fixed to the hook of the end of the tension transducer. The other end of the blood vessel was fixed to the calibration object. The vessel was immersed in Tyrode's solution at 37 °C. After fixing, the vessel began to generate information; the software interface displayed the tension level of the waveform. After a period of time, the blood vessels were soaked with Tyrode's solution containing SAA and SAA-30, and the vascular smooth muscle contraction signal was collected.

2.8. Electrocardiogram

Electrocardiograms were obtained using an MP150 (BIOPAC system, Inc., California, USA) with AcqKnowledge 4.0 software. ECG signal acquisition involves the use of an ECG100C amplifier. The ECG gain was set to 2000. The high pass filter was set to 0.05 Hz, and the low pass filter was set to 35 Hz OFF. The anesthetized mouse was injected with chloral hydrate before starting the procedure. The pad was heated to 40–42 °C to maintain a normothermic body temperature of 37 °C. Three needle electrodes were required for the experiment: a VIN+ connection of the left lower extremity, a right upper limb VIN- connection and a GND connection of the right lower extremity. A needle electrode was inserted into the subcutaneous tissues of each mouse. After setting raw channel and acquisition parameters, signal acquisition was initiated, and temperatures and ECG signals were recorded using AcqKnowledge 4.0 software.

2.9. Immunofluorescence probe co-localization

A cell climbing slice was prepared in a 24 well plate. When cells were attached to the wall, they were divided into a control group and salvianolic acid probe group. The cells were rinsed for 5 min with PBS buffer 3 times and then fixed in 3.7% formaldehyde at −4 °C for 10 min. The serum was diluted to 5% with room temperature PBS and incubated at room temperature for 30 min (closed liquid containing 0.1% Triton X-100). Primary antibodies used included rabbit anti-transgelin (dilution, 1:200; Abcam) and mouse anti-actin (dilution, 1:100; CST). After being rinsed gently with PBS three times, the cells were incubated at 37 °C for 1 h with Alexa Fluor® 488-conjugated goat anti-rabbit IgG (dilution, 1:150; KeyGEN BioTECH) and Alexa Fluor® 568-conjugated goat anti-mouse IgG (dilution, 1:250; Invitrogen) as secondary antibodies. The salvianolic acid probe was connected to 647 dyes by click reaction. The cells were viewed through a confocal microscopy system (Nikon, Japan).

2.10. Scanning electronic microscopy

This experiment involved a control group, SAA group and SAA-30 group. The concentration of SAA and SAA-30 was set to 10 μM. The cells were processed for SEM imaging immediately after the acquisition of confocal images. They were fixed with 4% glutaraldehyde in 0.1 M PBS for one hour, rinsed three times with 0.1 M PBS for 10 min and postfixed with 1% osmium tetroxide (OsO_4) in 0.1 M PBS for one hour. After removing the OsO_4 solution and rinsing is twice with bi-distilled water, the samples were gradually dehydrated by using an ethanol series in which ethanol was displaced with a gradient of TERT butanol and then dried using a vacuum dryer. Once dried, the samples were sputtered with gold (Polaron E5100 Sputter Coater, Bad Schwalbach, Germany), and images were acquired at 1–5 kV using a JCM-6000PLUS desktop scanning electron microscope (JEOL, Japan). Samples for the experiments described in Supplementary Fig. 6 were imaged before and after gold coating.

2.11. Negative staining electron microscopy

The copper mesh of the carbon film was subjected to hydrophilic treatment, and then 3 μL of the sample solution was placed on the carbon film and left there for one minute. Three sample solutions were used: actin; a mixture of actin and transgelin; and a mixture of actin, transgelin and salvianolic acid A. After excess sample liquid from the copper edge was removed with a filter paper, a drop of phosphotungstic acid dye was added, was left there for 1 min and was then air-dried at room temperature after the excess dye had been siphoned off. The dyed protein samples were observed under a freeze transmission electron microscope.

2.12. F-actin length statistics

AngioTool tracing in red of F-actin and in blue for branch points enabled a quantitative assessment of the vessel parameters. The F-actin area of SAA was significantly larger than that of the control group. The control group was significantly shorter in overall length. At the same time, the junction density in the SAA group was greater and the mean

E lacunarity of SAA was lower than those of the control group. Scale bars: All graphs show the mean ± SEM.

2.13. Calcium clamping of smooth muscle cells

The buffer solution was created by mixing 10 mmol/L EGTA with a certain Ca^{2+}-containing solution according to Ca^{2+}-EGTA stability constant K. The cytoplasmic Ca^{2+} concentration can be set to a desired level by the influx of buffer solution into the cytoplasm. This technique can be used to identify any agonist-initiated mechanisms that may modulate contractions without changing cytoplasmic Ca^{2+} levels. We set the Ca^{2+} concentration to the level determined to be optimal in the literature: pka = 6.3 [12]. Three groups were used: a control group, an SAA group (10 μM) and an SAA-30 group (10 μM). Then, the immunofluorescence staining of transgelin and actin within cells was performed and imaged using a confocal microscope (Nikon, Japan).

2.14. Biacore

The experiments were carried out using Biacore S200 SPR sensors (Biacore) with control software version 3.0 and Sensor Chip CM5 (carboxymethylated dextran surface). All assays were carried out at 25 °C.

Actin was immobilized via amine groups in all four available flow cells. First, the chip surface was activated following standard EDC/NHS protocol 11 with Biacore PBS-EP buffer used as the running buffer. Actin at a concentration of 0.4 mg/mL in 10 mM phosphate buffer pH 7.4 was then injected for 12 min followed by a 7 min injection of 1 M ethanolamine pH 8.5 to inactivate residual active groups. Typically, approximately 4000 RU of actin was immobilized per flow cell. By reference to the coupling steps of actin protein, transgelin protein was coupled to the chip. Preparation of SAA solution, The insoluble residue was pelleted by centrifugation and discarded. SAA was injected into the protein channel and blank channel at concentrations of 0 uM, 1.5625 uM, 3.125 uM, 4.6875 uM, 6.25 uM, 12.5 uM, 18.75 uM and 25 uM, respectively. The supernatant (200 μL) was injected at a flow rate of 20 μL/min. The protein binding period was set to 3 min, and the dissociation period was set to 300 s. The chip was regenerated with glycine-HCl (pH 2.5, 10 mM).

2.15. Statistics and reproducibility

Three independent experiments were performed using HVSMCs. Error bars represent the mean ± SEM. Statistical analyses were performed using Graph Pad Prism software. A two-tailed Student's *t*-test was used to evaluate differences between two groups of data, and the differences among the groups were analyzed by one-way ANOVA.Differences were considered significant when $^{*}p < .05$ or $^{**}p < .01$.

3. Results

3.1. Chemical synthesis and target identification of SAA

To improve the synthesis yield, we carried out a total synthesis of SAA. The synthetic route and steps of SAA are shown in Fig. S1. The full synthesis of SAA involved high levels of stereo selectivity (ee > 97%) and generated high yields (21% in total). Strong functional group tolerance was observed, deeming this a potentially excellent protocol for the synthesis of SAA derivatives. The purity of the SAA synthesized was measured as 98%. To identify protein targets that directly interact with SAA in cells, a SAA-probe was synthesized by reacting methyl-SAA with 3-Butyn-1-amine to form a methyl-SAA-probe, which was then demethylated with BBr_3 to form the SAA-probe (Fig. 1A & Fig. S2). The linker unit of a probe should be small enough to ensure that probe linkage takes place and to faithfully mimic noncovalent interactions occurring within live cells. In this way a small terminal alkyne handle was added to SAA to initiate pull-down reactions with biotin-N_3 via click chemistry. SAA-probe activity was measured through the calcium clamping of smooth muscle cells as described previously [12]. Despite structural derivatizations, the SAA probe enhanced the contraction of smooth muscle cells as effectively as the native compound (Fig. 1B).

To identify these target proteins, we performed target identification experiments using the SAA-probe in the HVSMC cell lines (Fig. 1C). In brief, the SAA-probe was incubated with growing cells. The SAA-probe was internalized and bound to its cellular targets in a dose-dependent manner with a positive correlation between the target protein concentration and probe concentration. The probe-binding proteins were conjugated with azide-biotin, enriched on streptavidin beads, and finally subjected to trypsin digestion. By liquid chromatography tandem mass spectrometry (LC-MS/MS), proteins captured by the SAA probe were identified. All of the proteins identified are listed in Table S1. Six proteins were identified as potential targets of SAA. Molecular docking was employed to evaluate the binding strength of SAA for the proteins. The results showed that Transgelin (TAGLN) presents the highest docking score (Fig. 1D). Consistently, cotreatment with siRNA of transgelin significantly impaired effects of SAA (Fig. 1E). These results collectively suggest that transgelin-controlled vascular smooth muscle cells are responsible for contraction effects of SAA.

3.2. SAA directly interacted with transgelin and actin

Using the SAA-probe we determined that transgelin and actin may be molecular targets of SAA. Biacore and microscale thermophoresis (MST) experiments were performed to validate whether SAA binds to transgelin and actin [13–16]. SAA was directly bound to transgelin in a concentration-dependent manner with micromolar binding affinity (KD = 7.11 μM) (Fig. 1F). A microscale thermophoresis analysis reveals a similar binding affinity value for SAA and transgelin (Fig. 1G). Synchrotron radiation small angle diffraction data show that SAA can lead to the conformational alteration of transgelin (Fig. S3). Similarly, SAA was bound to actin in a concentration-dependent manner (Fig. 1H). SAA promoted interaction between transgelin and actin as confirmed by Biacore analysis (Figs. 1I & 1J). Binding and stability assays show that protein binding signal values were 1.3 times greater when SAA was added (disregarding the effect of SAA). The tri-colour co-location experiments and confocal immunofluorescence imaging results reveal high SAA-probe, transgelin and actin levels in cells (Fig. 1K). Via stochastic optical reconstruction microscopy (STORM) we observed the co-localization of the SAA-probe with transgelin and actin distributed along the microfilament [17]. Furthermore, we compared F-actin features of the SAA and control groups (Fig. 1L). Compared to those of the control group, the F-actin area, F-actin percentage area, total F-actin length and average F-actin length increased in the SAA group (red is used to denote F-actin and blue is used to denote branch points for the quantitative assessment of F-actin parameters), showing that SAA regulates the stability and organization of the actin cytoskeleton by inducing filamentous actin bundling [18,19]. As the assembly of globular (G)-actin into F-actin and parallel stress fiber bundles continued, the mean E lacunarity (mean F-actin gap) was reduced. Thus, we hypothesized that SAA may enhance cell contraction effects by directly causing transgelin and actin to accelerate actin bundling in HVSMCs.

3.3. Designing SAA derivatives based on "rope" theory

To examine the binding of SAA to active sites of the transgelin-actin complex, molecular docking was performed. The results show that SAA promotes stable interactions of transgelin and actin complexes such as a "rope" the connects transgelin and actin (Fig. 2A). Two hydrogen bonds of SAA interact with Arg177 and Pro172 in actin, and two hydrogen bonds interact with Val42 and Glu28 in transgelin. SAA links key amino acids of the transgelin-actin complex through hydrogen bonding.

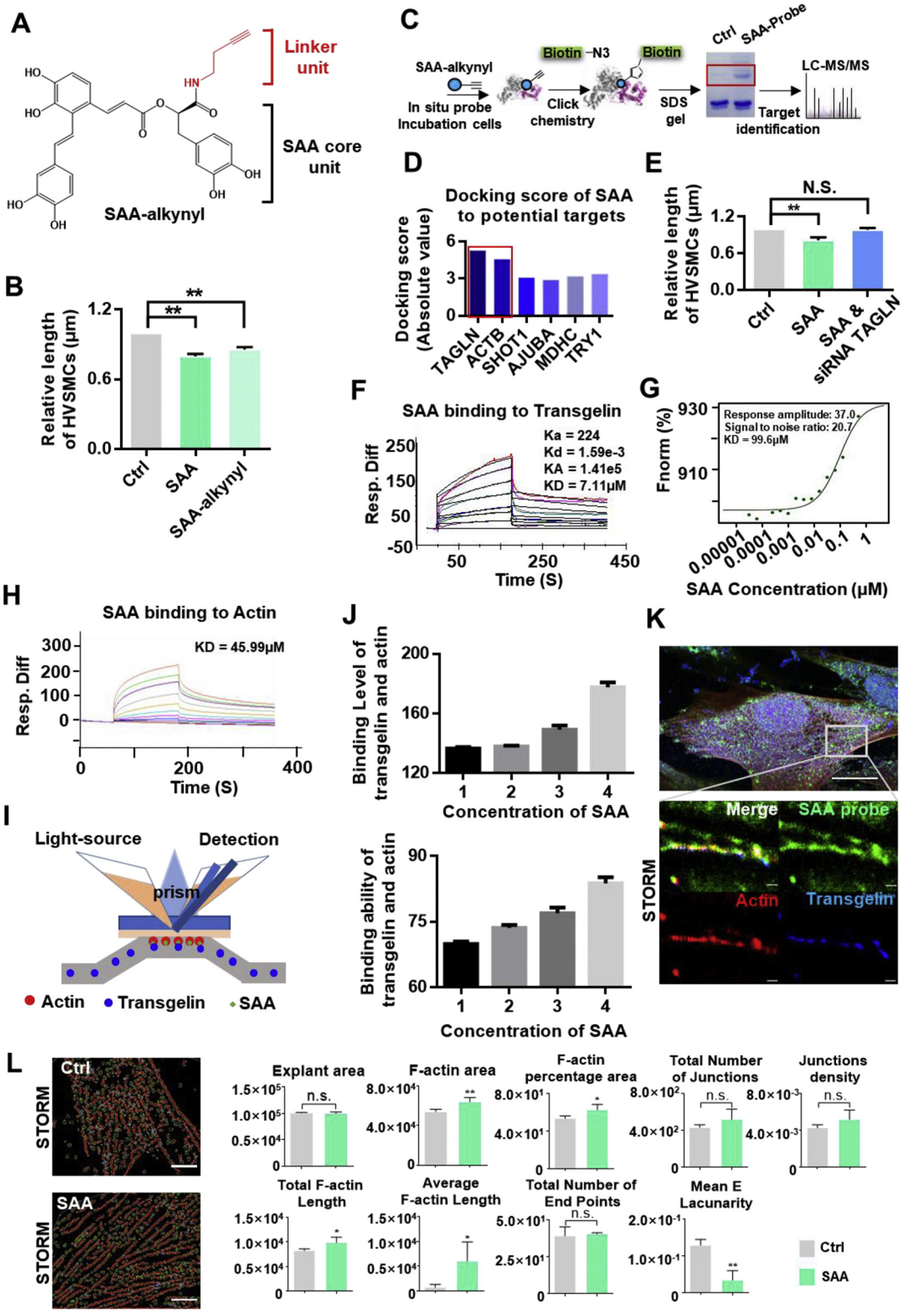

Fig. 1. Chemical probe synthesis, target identification and validation of SAA. (A) Structure of the SAA probe. The alkyne reporter group is shown in red. (B) Evaluation of the capacity of the SAA probe to enhance contraction effects in HVSMCs. (C) Overall scheme of the SAA probe target-captured experiments for identifying SAA targets. (D) Molecular docking scores of SAA bonds to six potential targets. (E) The cotreatment of transgelin siRNA counteracted the effect of SAA in enhancing contraction effects in HVSMCs. (F) Biacore analysis of SAA bonds to transgelin. Concentrations of SAA were set to 0 μM, 1.5625 μM, 3.125 μM, 4.6875 μM, 6.25 μM, 12.5 μM, 18.75 μM and 25 μM. The equilibrium dissociation constant (KD) was set to 7.11 μM. (G) Microscale thermophoresis analysis of SAA bonds to transgelin. (H) Biacore analysis of SAA bonds to actin. (I) A diagram of the Biacore analysis on how SAA promotes the interaction of transgelin according to actin experiments. (J) Binding levels and stability analysis results show that protein binding signal values of transgelin and actin were increased when SAA was added. (K) N-STORM images of SAA bound to transgelin and actin. These results show that single molecules of SAA bound to transgelin and actin, and structural information for the image shows that SAA and transgelin were distributed along with F-actin. (L) F-actin features for the control and SAA-treated groups. N.S., not significant. For all data, N.S. denotes no significance, $^{*}P < .05$, $^{**}P < .01$ ($n = 3$).

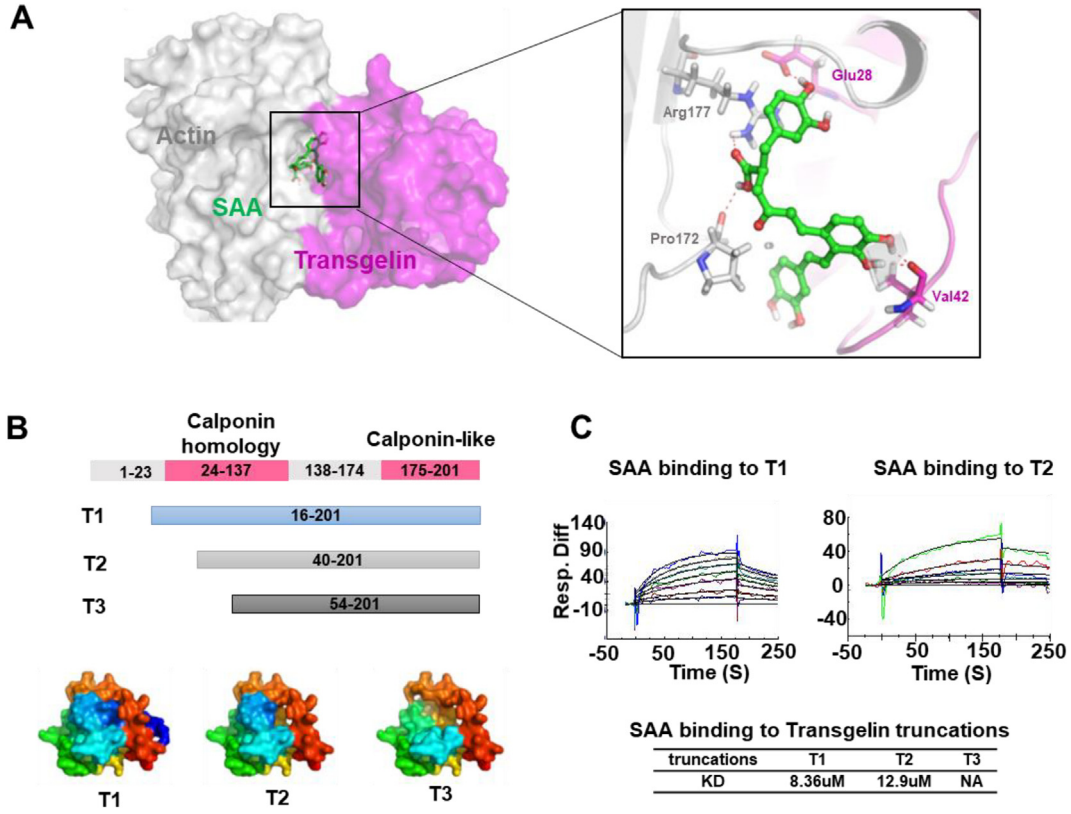

Fig. 2. Transgelin truncation and Biacore assay verification of key amino acid residues that interacted with SAA. (A) The binding mode of SAA at the protein interaction interface of the transgelin and actin complex. The results show that SAA directly targets bonds and "ropes" the transgelin-actin complex. (B) Three constructs of transgelin truncations were prepared. Transgelin truncation domains were modeled using Pymol software. (C) The Biacore binding assays show that SAA binds T1 and T2 at comparable levels while SAA cannot bind T3.

The stability and remoldability of the actin cytoskeleton were enhanced by the SAA-transgelin-actin complex. This prediction was validated by Biacore assays. Based on molecular docking patterns and protein structures, we prepared and purified protein truncation including T1 (16–201), T2 (40–201) and T3 (54–201) (Fig. 2B). The results show that SAA interacted with T1 and T2 but lost activity to T3 (Fig. 2C). Due to truncation, T2 became less active than T1. For T3, when a fragment of 1–53 was removed, SAA could no longer bind to transgelin.

Based on the binding model of SAA to the transgelin-actin complex, we divided SAA into two parts: the lock and linker. The lock is the phenolic hydroxyl of SAA that forms the hydrogen bond to transgelin and actin. The linker refers to carbon chains that link different aryl groups. Therefore, SAA was modified two ways by changing the rigidity or length of the linker and by increasing or decreasing the strength of the hydrogen bond. Based on this design strategy, compounds were designed and synthesized, and their activity was evaluated via Biacore. First, we synthesized 14 compounds based on a preliminary optimization strategy. SAA-1, SAA-2 and SAA-3, in converting double bonds to single bonds, declined more than four-fold in terms of transgelin activity relative to SAA. Thus, double bonds are central to maintaining configurations of SAA links and activity (Fig. 3A). A comparison of SAA-4, SAA-5, and SAA-6 to SAA shows that their binding affinities were reduced to 3650 μM or to no activity. Thus, the length of the linker cannot be increased, and the length of SAA may be the appropriate length for the interface of the transgelin-actin complex (Fig. 3B). Given synthetic difficulties associated with SAA, SAA-7, SAA-8, and SAA-9 were synthesized. The carboxyl group is known as essential to binding; when the carboxyl group was changed to an ester group, bioactivity levels increased to 5.06 μM (Fig. 3C). When we compared SAA-10, SAA-11, SAA-12, SAA-13, and SAA-14 to SAA, we found that the meta-hydroxyl group of the *danshensu* part of the molecule was essential in locking the target and that the para-hydroxyl group of the *danshensu* part of the molecule may experience steric hindrance (Fig. 3D). Based on preliminary structure-activity relationships of SAA-1 through SAA-14, we designed a second collection of SAA derivatives. SAA-3 with a carboxyl group changed to an ester group and with no para-hydroxyl group in the *danshensu* part of the molecule exhibiting stronger binding affinity to transgelin with a KD value of 2.39 μM (Fig. 3E). The synthesis and characterization of these compounds are presented in our supplementary data, and our activity test results are shown in Table S2.

To better understand factors that enhanced SAA-30 activity, structural energy levels were measured (Fig. 4A). Stretch, bend, torsional and van der Waals energy levels for SAA-30 were found to be lower than those of SAA, showing that SAA-30 is more structurally stable. Biacore results for SAA-30 bonds to transgelin are shown in Fig. 4B. Compared to that of SAA, SAA-30 presents a higher docking score of −7.105, more stable binding energy levels (−21.692 kcal/mol) and a better fitting mode to the transgelin-actin complex (Figs. 4C-4D & Table S3). In summary, we obtained a preliminary structure-activity relationship for SAA according to which the rigidity and length of links are essential and whereby changing the carboxyl group to an ester group increases its lipid solubility; the para-hydroxyl group of the *danshensu* part of the molecule may be more suitable as a lock.

3.4. SAA and SAA-30 promoted cell contractions by facilitating the aggregation of actin in vitro

To characterize the actin cross-linking activity of SAA and SAA-30, we employed multi-angle laser scattering to measure the aggregation of the actin filament in the presence or absence of SAA and SAA-30. The results show that when transgelin was added, the polymerization of actin was enhanced and then further enhanced by SAA and SAA-30 (Fig. 5A). By negative staining electron microscopy we also examined actin filaments in the presence and absence of SAA and SAA-30. In the

A

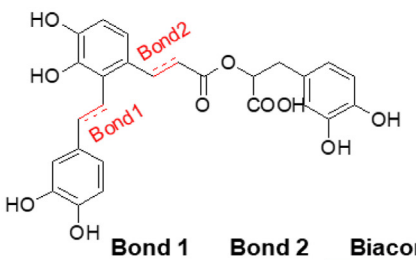

	Bond 1	Bond 2	Biacore (μM)
SAA	double	double	7.11
SAA-1	double	single	21.9
SAA-2	single	double	19.2
SAA-3	single	single	31.2

B

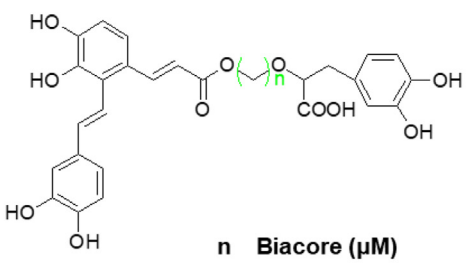

	n	Biacore (μM)
SAA-4	1	NA
SAA-5	2	3650
SAA-6	4	NA

C

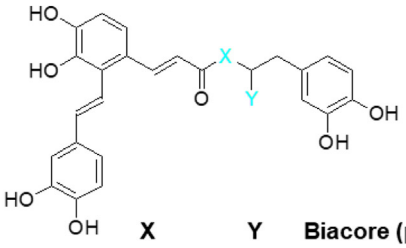

	X	Y	Biacore (μM)
SAA-7	NH	COOH	41.4
SAA-8	O	COOEt	5.06
SAA-9	O	N/A	NA

D

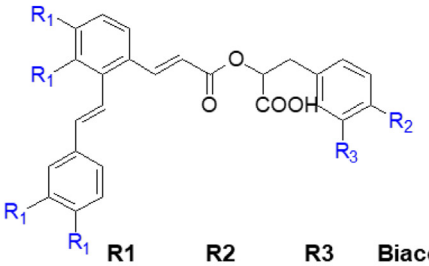

	R1	R2	R3	Biacore (μM)
SAA-10	OH	N/A	N/A	NA
SAA-11	OH	OH	N/A	48.9
SAA-12	OH	N/A	OH	16.6
SAA-13	OMe	OMe	OMe	40.9
SAA-14	OMe	OH	OH	35.4

E

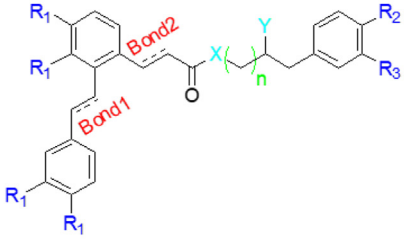

	Bond 1	Bond 2	n	X	Y	R1	R2	R3	Biacore (μM)
SAA	double	double	0	O	COOH	OH	OH	OH	7.11
SAA-15	double	double	0	OH	NA	NA	NA	NA	6.62
SAA-16	NA	double	0	O	COOH	OH	OH	OH	14
SAA-17	double	double	0	O	COOEt	OMe	NA	OMe	NA
SAA-18	single	single	0	O	COOEt	OMe	NA	OMe	NA
SAA-19	single	single	0	O	COOEt	OMe	NA	NA	41.4
SAA-20	double	double	2	NH	COOEt	OMe	NA	OMe	110
SAA-21	double	double	2	NH	COOEt	OMe	NA	NA	NA
SAA-22	single	single	2	NH	COOEt	OMe	NA	OMe	NA
SAA-23	single	single	4	NH	COOEt	OMe	NA	OMe	NA
SAA-24	single	single	4	NH	COOEt	OMe	NA	NA	72.4
SAA-25	single	single	2	NH	COOEt	OH	NA	OH	602
SAA-26	single	single	2	NH	COOEt	OH	NA	NA	742
SAA-27	double	double	4	NH	COOEt	OMe	NA	OMe	NA
SAA-28	double	double	2	NH	COOH	OMe	NA	OMe	NA
SAA-29	double	double	0	NH	NA	NH_2	NH_2	NH_2	NA
SAA-30	double	double	0	O	COOEt	OH	NA	OH	2.39
SAA-31	double	double	0	NH	COOEt	OH	NA	NA	NA
SAA-32	single	single	0	NH	COOEt	OH	NA	OH	NA
SAA-33	single	single	0	NH	COOEt	OH	NA	NA	NA
SAA-34	double	double	2	NH	COOEt	OH	NA	OH	NA
SAA-35	double	double	2	NH	COOEt	OH	NA	NA	1350
SAA-36	double	double	4	NH	COOEt	OH	NA	OH	77.3
SAA-37	double	double	4	NH	COOEt	OH	NA	NA	191

Fig. 3. Optimized structures of SAA and synthesis of SAA derivatives. (A-E) Structures and active values of SAA derivatives. SAA optimization focused on the following: the length of the linker, the interaction strength of hydrogen bonds and the flexibility of the linker.

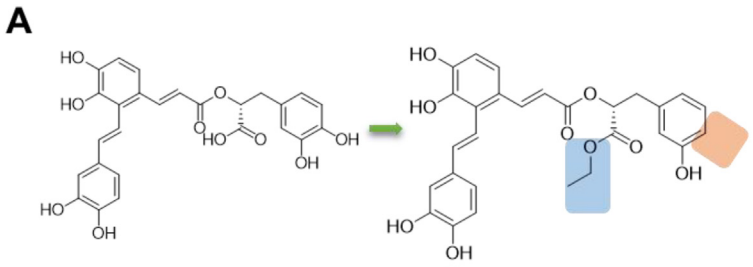

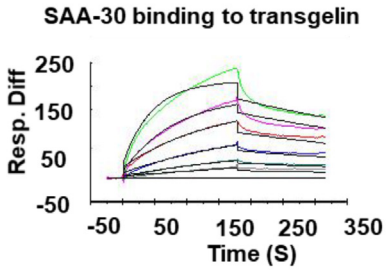

Concentration of SAA-30 (μM)	Req (RU)
0	0
1.5625	76.3
0.78125	47.6
3.125	109
6.25	140
12.5	162
25	176

Compound	Stretch Energy	Bend Energy	Torsional Energy	Improper Torsional Energy	Van der Waal Energy
SAA	9.423	23.512	49.882	0.241	76.112
SAA-30	9.320	19.354	44.174	0.324	74.077

Compound	Ka (1/Ms)	Kd (1/s)	KA (1/M)	KD (uM)
SAA	224	1.95e-3	1.41e5	7.11
SAA-30	816	1.95e-3	4.19e5	2.39

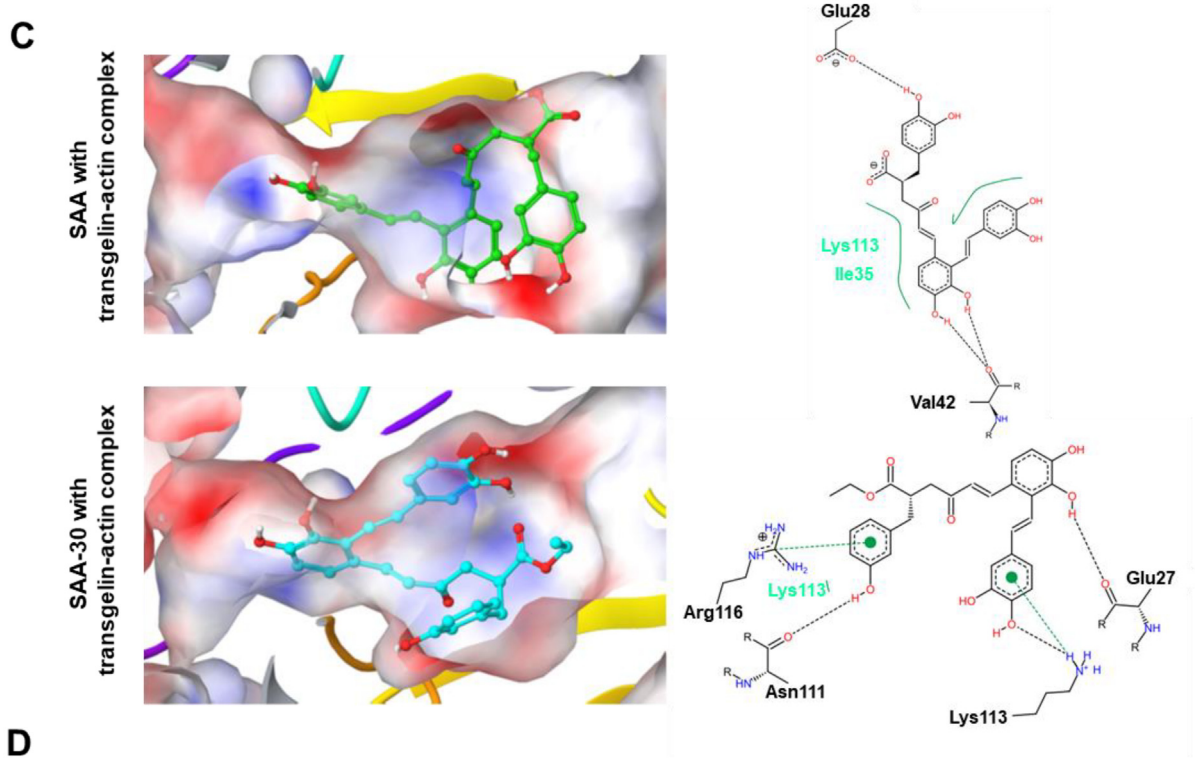

D

Protein	Compound	Docking Score	Binding energy (kcal/mol)	No. of hydrogen bonds	Hydrogen bond forming residues	Distance (Å)	Cation-π interactions	Hydrophobic interaction
Transgelin-actin complex	SAA	-6.286	-20.117	4	Pro172, Arg177, Glu28, Val42	2.7, 2.9, 1.8, 2.0	NA	Lys113, Ile35
	SAA-30	-7.105	-21.692	4	Glu107, Asn111, Lys113, Glu27	2.8, 2.2, 2.6, 1.8	Arg116, Lys113	Lys113

Fig. 4. Comparison of SAA and SAA-30 structural and binding modes. (A) The structural energy levels of SAA-30 was lower than that of SAA. (B) Biacore results for SAA-30 bound to transgelin. SAA-30 was three times more active than SAA. (C) The binding mode of SAA and SAA-30 in the active site of the transgelin and actin complex. SAA-30 generated a higher docking score of −7.105 relative to that of the transgelin-actin complex. The green dotted line denotes the cation-π interaction. The black dotted line denotes hydrogen bond interactions, and the green solid line denotes hydrophobic interactions. (D) Table showing docking scores, binding energy levels, hydrogen bond interactions, cation-π interactions and hydrophobic interactions between SAA and SAA-30 and the transgelin-actin complex. SAA-30 shows lower binding energy levels in the transgelin-actin complex than in the SAA.

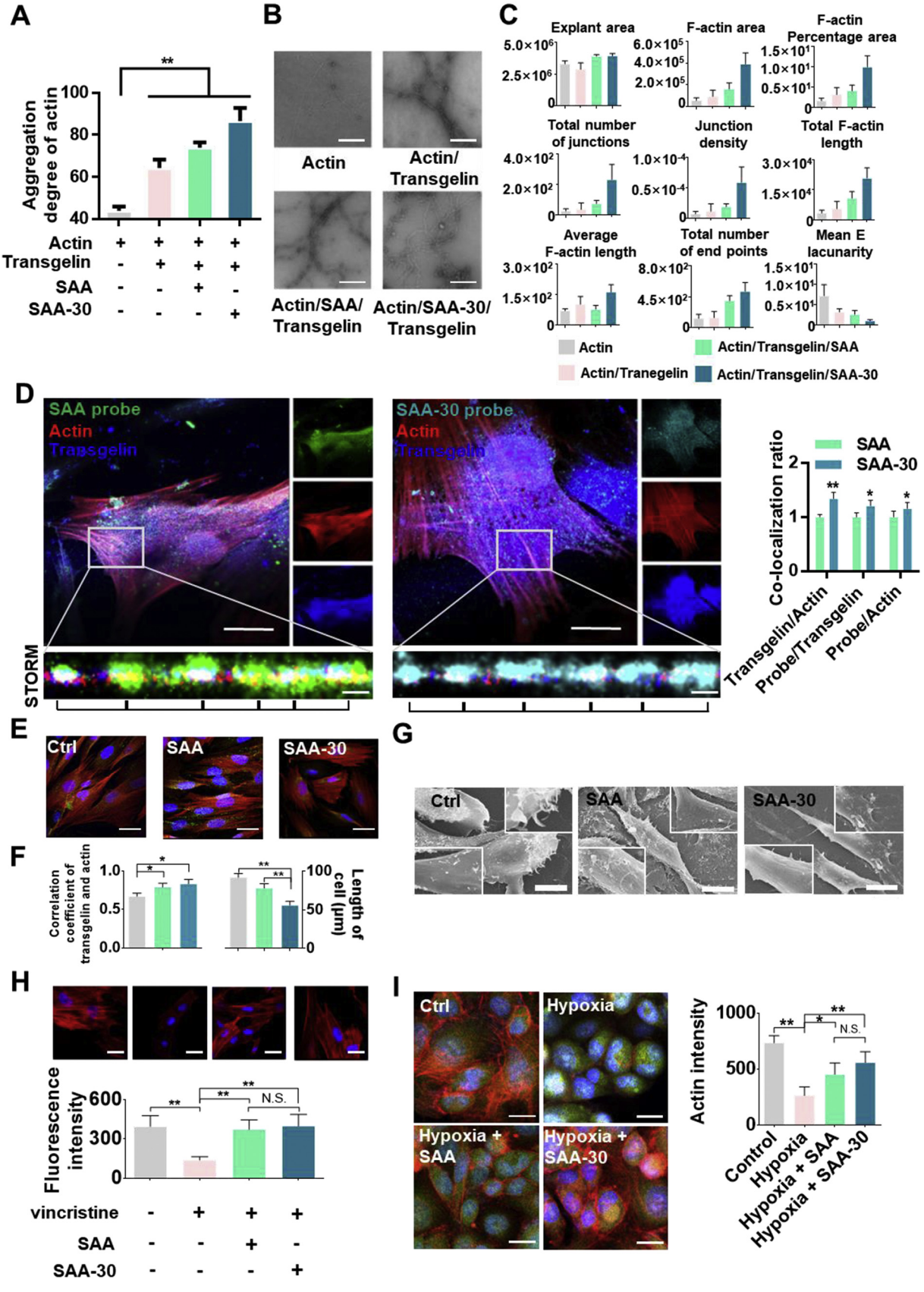
A
Aggregation degree of actin
Actin
Transgelin
SAA
SAA-30
B
Actin
Actin/ Transgelin
Actin/SAA/ Transgelin
Actin/SAA-30/ Transgelin
C
Explant area
F-actin area
F-actin Percentage area
Total number of junctions
Junction density
Total F-actin length
Average F-actin length
Total number of end points
Mean E lacunarity
Actin
Actin/Tranegelin
Actin/Transgelin/SAA
Actin/Transgelin/SAA-30
D
SAA probe
Actin
Transgelin
SAA-30 probe
STORM
Co-localization ratio
SAA
SAA-30
Transgelin/Actin
Probe/Transgelin
Probe/Actin
E
Ctrl
SAA
SAA-30
F
Correlation coefficient of transgelin and actin
Length of cell (μm)
G
Ctrl
SAA
SAA-30
H
Fluorescence intensity
N.S.
vincristine
SAA
SAA-30
I
Ctrl
Hypoxia
Hypoxia + SAA
Hypoxia + SAA-30
Actin intensity
N.S.
Control
Hypoxia
Hypoxia + SAA
Hypoxia + SAA-30

absence of transgelin, actin filaments were thin and short. In contrast, in the presence of transgelin, actin was polymerized, and in SAA and SAA-30 groups, there was a marked increase in actin polymerization. These results demonstrate that SAA stabilized actin filaments against disassembling and that SAA-30 was more active than SAA (Fig. 5B). The F-actin area, F-actin percentage area and total F-actin length were significantly increased in the SAA-30 group. The total number of junctions and junction density levels were increased and mean E lacunarity levels were decreased in SAA-30, meaning that filamentous actin bundling was promoted (Fig. 5C).

Single-molecule fluorescence imaging results show structural characteristics of SAA and SAA-30 bonds to the transgelin-actin complex. SAA and SAA-30 were uniformly distributed along microfilaments (Fig. 5D). This suggests that the organization of the actin cytoskeleton is regulated by SAA and SAA-30. To investigate whether SAA- and SAA-30-induced F-actin bundling regulates the contractility of vascular smooth muscle cells (VSMCs), we performed an immunofluorescence staining of actin and transgelin in living cells. SAA and SAA-30 increased VSMC contractility and reduced cell lengths in the calcium clamping assay, and the co-localization of transgelin and actin was enhanced. The average length of VSMCs changed from approximately 90 μm in the control group to 80 μm in the SAA group and to 60 μm in the SAA-30 group. The co-localization of transgelin and actin in the control group was measured as approximately 57% but this increased to 78% in the SAA group and to 83% in the SAA-30 group (Figs. 5E & 5F). When treated with SAA (10 μM) and SAA-30 (10 μM), the relative length of CASMCs declined while F-actin formation was enhanced. Thus, the effect of SAA and SAA-30 in promoting the contraction of CASMCs was also observed (Fig. S4). SEM results show that SAA and SAA-30 enhanced cell adherence and cell surface tension. Numerous microfilaments (tono-filaments) and desmosomes were observed in both the SAA and SAA-30 groups (Fig. 5G).

SAA and SAA-30 combatted the capacities of F-actin inhibitors and increased F-actin levels relative to the actin inhibitor group. Structures of F-actin were very thin and dispersed, and fluorescence intensity levels decreased from 395 to 139 in the vincristine treated group but increased to 373 in the SAA/vincristine group and to 398 in the SAA-30/vincristine group (Fig. 5H). SAA and SAA-30 also limited hypoxia-induced actin degradation. During MI, fibers and actin degraded and lost their functions. SAA and SAA-30 can protect muscle fibers and maintain their functions. The fluorescence intensity of the hypoxic group was measured as 264 but this increased to 453 in the SAA group and to 558 in the SAA-30 group. SAA-30 was more active than SAA (Fig. 5I). A gene set enrichment analysis also shows that SAA enhanced the aggregation of actin and the contraction of smooth muscle cells (Figs. S5-S7) [20].

3.5. SAA-30 better protected myocardial functions during myocardial ischemia than SAA in wild type mice; however, neither SAA nor SAA-30 had a therapeutic effect on transgelin (−/−) mice

To verify the agonism of SAA and SAA-30 on isolated blood vessels, we performed a muscle tension test (Fig. 6A). SAA-30 increased smooth muscle vessel tension more effectively than SAA in WT mice but inhibited agonism effects on transgelin knockout mice (Fig. 6B & Fig. S8). SAA had no stimulation effect on isolated myocardial tissue (Table S4). This may be the case because myocardial tissue does not express transgelin (Fig. S9). A diagram illustrating the generation of the MI model and the treatment schedule is shown in Fig. 6C. The electrocardiogram ST segment underwent marked changes in the isoproterenol-treated group, and the results show signs of acute myocardial ischemia in the model groups (Fig. S10). Compared to those of the normal mice, the heart rates of the MI mice increased by approximately 1.2 times and the ST segment changed by >0.25 mV (Fig. 6D). These ST segment changes and heart ratios were restored to nearly normal levels with an SAA-30 pretreatment of 10 mg/kg for 7 days (Fig. 6E). In the transgelin (−/−) group, SAA and SAA-30 had no therapeutic effect on myocardial ischemia. These results further verify that the target of SAA is transgelin. A histopathological examination clearly reveals organizational structures of the myocardium. The normal group included cardiac fibers without any infarctions, edema, inflammatory cells or necrotic regions. Heart tissue in the isoproterenol-treated group exhibited an infracted zone with edema, inflammatory cell infiltration and muscle fiber separation. The administration of 10 mg/kg SAA-30 protected heart tissue from ischemic injury and resulted in a decreased level of coagulated necrosis and in the presence of fewer infiltrating inflammatory cells (Fig. 6F and Fig. S11). The percentage of infarction (infarction ratio) for wild type MI mice was measured as 11.2% while that for transgelin (−/−) mice was measured as 16.2%. Heart infarction ratios of the SAA and SAA-30 groups of wild type mice were measured as 4% and 3.2%, respectively (Fig. 6G). We observed no myocardial protective effect of SAA-30 on the transgelin (−/−) mice. Compared to the normal group, the isoproterenol-treated group presented significantly increased levels of the following serum myocardial injury marker enzymes: creatine kinase (CK, 166% ± 14%), creatinine kinase MB isoenzyme (CK-MB, 165% ± 24%), aspartate transaminase (AST, 237% ± 19%) and lactate dehydrogenase (LDH, 174% ± 14%). Pretreatment with SAA-30 rather than SAA had a more obvious therapeutic effect on wild type MI mice and nearly restored levels of CK (112% ± 4%), CK-MB (105% ± 13%), AST (115% ± 10%) and LDH (123% ± 19%) to normal values. In the transgelin (−/−) group both SAA and SAA-30 had no therapeutic effect, and CK, CK-MB, AST and LDH levels were not significantly changed relative to those of the transgelin (−/−) MI model group (Fig. 6H). A schematic diagram of SAA and SAA-30 treatments of myocardial ischemia is presented in Fig. 6I.

4. Discussion

Myocardial ischemia blocks or limits blood flow to certain parts of the heart. Oxygen-derived free radicals are generated during myocardial ischemia-reperfusion (I/R), lipid peroxidation-derived unsaturated aldehydes accumulate, and variable angina and infarction can occur [21–23]. *Salvia miltiorrhiza* is a Chinese medicine commonly used to treat cardiovascular disease [24]. Salvianolic acids are water-soluble compounds of *Radix Salvia miltiorrhiza*. It has been reported that SAA serves as a potent scavenger of ROS during cardiovascular injury and inhibits the adherence of leukocytes to endothelial cells. In addition, SAA inhibits inflammation, regulates the expression of metalloproteinases

Fig. 5. SAA and SAA-30 increased cell contractions in vitro. (A) Multi-angle light scattering results show that the aggregated state of actin was enhanced when transgelin was added. SAA and SAA-30 further promoted actin aggregation. (B) Negative staining electron microscopy analysis of actin, actin/transgelin, actin/transgelin/SAA and actin/transgelin/SAA-30 groups. The results show that transgelin enhanced actin polymerization, which was further markedly enhanced by SAA and SAA-30. SAA-30 was the most active. (C) Quantitative analysis of F-actin. The F-actin area, F-actin percentage area and total F-actin length were increased when transgelin was added. SAA and SAA-30 further promoted actin aggregation. (D) Accurate multidirectional co-localization analysis of SAA probes and of SAA-30 probe interactions with transgelin and actin via confocal and N-STROM. Green, SAA probe; Cyan, SAA-30 probe; Red, Actin; Blue, Transgelin. The results show the structural characteristics of SAA and SAA-30 bound to transgelin and actin. SAA and SAA-30 were distributed along with the transgelin-actin complex and promoted the uniform distribution of actin. (E & F) SAA and SAA-30 promoted the co-localization of transgelin and actin and cell contractions. Actin is shown in red and transgelin is shown in green. (G) The SEM results show that SAA and SAA-30 enhanced HVSMC contractility levels. Cytoskeletons were clearly aggregated, and their adhesion capacities were enhanced. Cells were assayed after treatment with 20 μM SAA and SAA-30 for 24 h. (H) SAA and SAA-30 combatted inhibition by an actin inhibitor. The depolymerization capacities of actin inhibitor were antagonized by SAA and SAA-30. (I) SAA and SAA-30 limited hypoxia-induced actin degradation. Results were obtained from three independent experiments with each experiment performed in triplicate; N.S. denotes no significance, and error bars represent standard deviations ($^{*}P < .05$, $^{**}P < .01$). Data are presented as mean ± SEM values.

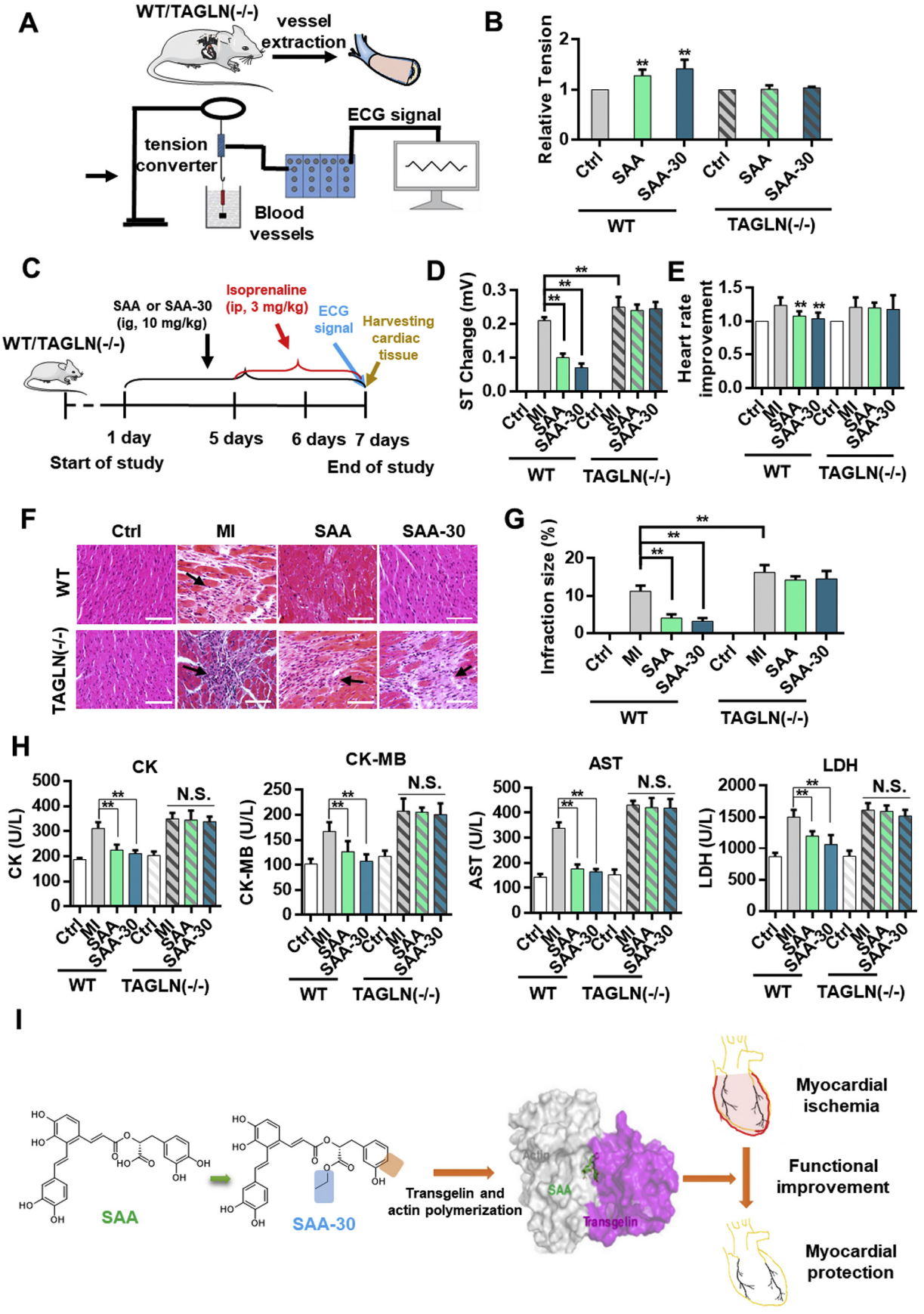
A
WT/TAGLN(-/-)
vessel extraction
ECG signal
tension converter
Blood vessels
B
Relative Tension
Ctrl
SAA
SAA-30
WT
TAGLN(-/-)
C
SAA or SAA-30 (ig, 10 mg/kg)
Isoprenaline (ip, 3 mg/kg)
ECG signal
Harvesting cardiac tissue
WT/TAGLN(-/-)
1 day
5 days
6 days
7 days
Start of study
End of study
D
ST Change (mV)
E
Heart rate improvement
MI
F
Ctrl
MI
SAA
SAA-30
WT
TAGLN(-/-)
G
Infraction size (%)
H
CK
CK-MB
AST
LDH
CK (U/L)
CK-MB (U/L)
AST (U/L)
LDH (U/L)
N.S.
I
SAA
SAA-30
Transgelin and actin polymerization
Actin
Transgelin
Myocardial ischemia
Functional improvement
Myocardial protection

during cardiovascular injury and improves coronary artery functioning and coronary microcirculation [4,25–27].

While several semi-synthesis procedures and total SAA synthesis methods have been developed, they apply to milligram production levels. Here we propose a novel approach to the total synthesis of SAA. The method optimizes the total synthetic process and increases SAA yields to the gram level. We have also optimized the structure of SAA using a series of structural derivatives based on this simple method, which includes the SAA-probe.

We have developed a cell-permeable probe capable of profiling potential cellular targets of SAA. Specifically, careful consideration was made to maintain the integrity of noncovalent interactions of SAA and targets in the design of our SAA probe. In this way, SAA activity was maintained. In comparing results of LC-MS/MS and molecular docking results we found that transgelin and actin may act as targets of SAA. We further used single-molecule imaging, Biacore assays and microscale thermophoresis experiments to identify transgelin and actin as targets of SAA. Transgelin, an actin-binding protein, interacts with actin and promotes actin aggregation [28,29]. Transgelin is highly expressed in smooth muscle cells (Fig. S8) [30]. From three elements of a composite Biacore assay we found that SAA enhances the interaction of transgelin with actin. SAA significantly enhanced microfilament protein aggregation in vitro. SAA linked transgelin and actin interactions like a rope. Biacore assays of protein truncates further verify molecular docking results. In analyzing the binding mode of SAA we designed and synthesized a series of SAA derivatives. By comparing activities of the derivatives we investigated structure-activity relationships (SAR) of SAA derivatives and of the transgelin-actin complex. First, the rigidity of the linker proved essential in maintaining the complex configuration. Changing the molecular rigidity of SAA may cause the compound to fail to interact with key amino acid residues of the transgelin-actin complex, preventing the stability of the composite from being maintained. Second, the length of the linker cannot be increased or decreased. According to the pocket shape of the transgelin-actin complex, the length of SAA linkers may be best suited for binding. Third, while the carboxyl group proved essential, by changing the carboxyl group to an ester group to increase lipid solubility we found that bioactivity levels were also enhanced. Finally, the meta-hydroxyl group of the *danshensu* part of SAA proved essential for locking the target while the para-hydroxyl group of the *danshensu* part may be sterically hindered. Based on the SAR we designed and synthesized SAA-30. The KD value of SAA-30 was found to be three times greater than that of SAA. Compared to SAA, SAA-30 is more structurally stable and more effectively binds to the transgelin-actin complex. SAA-30 stabilized actin filaments against disassembling and increased the rigidity of actin filaments [31]. The rigidity of the actin filaments increases the contractility of coronary vascular smooth muscle, limits F-actin degradation under hypoxia and shortens the functional refractory period.

The basic components of arterial vessels include endothelial cells, vascular smooth muscle cells and extracellular matrixes. These three basic components forms the three-layer loop structure of arterial vessels, including the inner, middle and outer membranes. Vascular smooth muscle cells form the main cellular components of blood vessel walls and maintain vascular tone. Vasoconstriction is mainly caused by vascular smooth muscle. As vasosmooth muscle contracts, blood vessels constrict. In VSMCs, in addition to maintaining a certain cell morphology, the cytoskeleton is also involved in the contractile activity of VSMCs. Transgelin is mainly expressed in vascular smooth muscle cells. As a regulatory protein of the cytoskeletal structure, transgelin participates in cytoskeletal remodeling by promoting the polymerization of G-actin protein into F-actin cross-linking. Therefore, transgelin is closely related to the contractile functions of smooth muscle cells. The experimental results show that knocking out transgelin expands the area damaged by atherosclerosis [32]. Transgelin can also affect the development of atherosclerosis by regulating the vascular smooth muscle phenotype [11]. Therefore, drug development targeting transgelin and the regulation of cell contraction activity and robustness are essential to treatment and drug research on myocardial ischemia. Acute myocardial ischemia is severely harmful to human health, and its pathogenesis remains unclear [33]. The isoproterenol-induced cardiotoxic effect is described in an animal model that may be used to study pathology and drug development [34–42]. Here, SAA-30 had clearly stronger cardioprotective effects than SAA against isoproterenol-induced myonecrosis, improved the ST segment of the electrocardiogram, increased coronary blood flow volumes and restored serum myocardial injury marker enzymes to near normal levels. CK, CK-MB, AST and LDH are marker enzymes for MI and can reflect levels of myocardial injury [43–45]. SAA and SAA-30 maintain the integrity of myocardial cells, thereby preventing the leakage of these diagnostic marker enzymes into serum. During MI, increased ROS levels cause the formation of necrotic lesions and severely impair cellular functions. There are two hydroxyl groups on the benzene ring of SAA and SAA-30. The structural characteristics of SAA and SAA-30 may involve the scavenging of oxygen free radicals.

SAA-30 is safe to use, and biochemical indexes of liver and kidney function were not significantly changed with or without SAA-30 use in normal mice (Table S5). The results of the acute toxicity experiment show that an oral lethal median dose of SAA-30 used in mice is >2 g/kg body weight (MTD > 2 g/kg). Long-term toxicity tests show no other abnormal effects on the weight, behavior, blood and biochemical indexes, organ coefficients and organ pathology of the SAA-30 and control groups (Fig. S12).

In this study, we analyzed target identification results obtained from an LC-MS/MS of an SAA probe and found that our clickable probe can identify SAA targets. Furthermore, we observed functional interactions occurring between transgelin and actin with important implications for the myocardial protection of MI. The therapeutic targeting of the transgelin/actin complex and the "rope" drug design method for modulating vascular smooth muscle contractions are of clinical translational research value in terms of treating MI. Mechanisms of action of the transgelin/actin complex and of SAA-30 may also contribute to other diseases associated with IR tissue injury.

Acknowledgements

This study was supported by the National Natural Science Foundation of China (grant nos. 81572838, 81402973, and 81703581), Tianjin Natural Science and Technology Fund (grant no. 15JCYBJC26400), Tianjin Science and Technology Project (grant no. 15PTGCCX00140), and the National Science and Technology Major Project (grant no. 2017ZX09306007).

Competing interests

The authors declare no conflict of interest.

Fig. 6. SAA-30 promoted the contractility of vascular smooth muscle cells more than SAA and better achieved myocardial protection than SAA. (A) Overall scheme of muscular tension agonistic effects of SAA and SAA-30 on WT and transgelin (−/−) mice. (B) SAA and SAA-30 enhanced contractile capacities of vascular smooth muscle in isolated vascular smooth muscles of WT mice. (C) Diagram illustrating the generation of the MI model and the treatment schedule. (D) ST changes and (E) heart rate improvements observed in WT and transgelin (−/−) mice after IR injury with or without SAA and SAA-30 treatment. (F) Histopathological changes and (G) infraction sizes observed in MI-injured hearts of WT or transgelin (−/−) mice with or without SAA and SAA-30 administration. (H) Measurement of CK, CK-MB, AST and LDH levels in WT and transgelin (−/−) mice after IR injury with or without SAA and SAA-30. (I) A schematic diagram of SAA and SAA-30 treatments of myocardial ischemia. $^{*}P < .05$, $^{**}P < .01$ ($n = 6$). N.S., not significant. Data are represented as mean ± SEM values.

Author contributions

Tao Sun and Cheng Yang designed research. Weilong Zhong, Bo Sun, Longcong Huai, Lingfei He, Yuan Liang, Honglian Tao, Yuanhao Tang, Wei Yang performed research and analyzed data. Wenqing Gao, Shuang Chen, Yanrong Liu, Huijuan Liu, Heng Zhang, Yuan Qin, Lan Yang, Honggang Zhou performed data analysis. Weilong Zhong, Bo Sun, Lingfei He, Xiaoyun Zhang wrote the paper, with contributions from all authors. All authors have read and approved the final manuscript.

Appendix A. Supplementary data

Supplementary data to this article can be found online at https://doi.org/10.1016/j.ebiom.2018.10.041.

References

[1] Liu J, Kuang P, Wu W, et al. Radix Salviae miltiorrhizae protects rat hippocampal neuron in culture from anoxic damage. J Tradit Chin Med 1998;18(1):49–54.
[2] Wang X, Morris-Natschke SL, Lee KH. New developments in the chemistry and biology of the bioactive constituents of Tanshen. Med Res Rev 2007;27(1):133–48.
[3] Zhou L, Zuo Z, Chow MS. Danshen: an overview of its chemistry, pharmacology, pharmacokinetics, and clinical use. J Clin Pharmacol 2005;45(12):1345–59.
[4] Ho JH, Hong CY. Salvianolic acids: small compounds with multiple mechanisms for cardiovascular protection. J Biomed Sci 2011;18:30.
[5] Liu M, Li YG, Zhang F, et al. Chromatographic fingerprinting analysis of Danshen root (Salvia miltiorrhiza Radix et Rhizoma) and its preparations using high performance liquid chromatography with diode array detection and electrospray mass spectrometry (HPLC-DAD-ESI/MS). J Sep Sci 2007;30(14):2256–67.
[6] Wang MX, Liu YY, Hu BH, et al. Total salvianolic acid improves ischemia-reperfusion-induced microcirculatory disturbance in rat mesentery. World J Gastroenterol 2010;16(42):5306–16.
[7] Fan H, Yang L, Fu F, et al. Cardioprotective effects of salvianolic acid A on myocardial ischemia-reperfusion injury in vivo and in vitro. Evid Based Complement Alternat Med 2012;2012 (508938).
[8] Yuan X, Xiang Y, Zhu N, et al. Salvianolic acid A protects against myocardial ischemia/reperfusion injury by reducing platelet activation and inflammation. Exp Ther Med 2017;14(2):961–6.
[9] Chen Q, Xu T, Li D, et al. JNK/PI3K/Akt signaling pathway is involved in myocardial ischemia/reperfusion injury in diabetic rats: effects of salvianolic acid A intervention. Am J Transl Res 2016;8(6):2534–48.
[10] Han M, Dong LH, Zheng B, Shi JH, Wen JK, Cheng Y. Smooth muscle 22 alpha maintains the differentiated phenotype of vascular smooth muscle cells by inducing filamentous actin bundling. Life Sci 2009;84(13–14):394–401.
[11] Shen J, Yang M, Jiang H, et al. Arterial injury promotes medial chondrogenesis in Sm22 knockout mice. Cardiovasc Res 2011;90(1):28–37.
[12] Si XM, Huang L, Paul SC, An P, Luo HS. Signal transduction pathways mediating CCK-8S-induced gastric antral smooth muscle contraction. Digestion 2006;73(4):249–58.
[13] Wienken CJ, Baaske P, Rothbauer U, Braun D, Duhr S. Protein-binding assays in biological liquids using microscale thermophoresis. Nat Commun 2010;1:100.
[14] Seidel SA, Wienken CJ, Geissler S, et al. Label-free microscale thermophoresis discriminates sites and affinity of protein-ligand binding. Angew Chem Int Ed Engl 2012;51(42):10656–9.
[15] Casper D, Bukhtiyarova M, Springman EB. A Biacore biosensor method for detailed kinetic binding analysis of small molecule inhibitors of p38alpha mitogen-activated protein kinase. Anal Biochem 2004;325(1):126–36.
[16] Cannon MJ, Papalia GA, Navratilova I, et al. Comparative analyses of a small molecule/enzyme interaction by multiple users of Biacore technology. Anal Biochem 2004;330(1):98–113.
[17] Zhuang X. Nano-imaging with Storm. Nat Photonics 2009;3(7):365–7.
[18] Sawaguchi S, Varshney S, Ogawa M, et al. O-GlcNAc on NOTCH1 EGF repeats regulates ligand-induced notch signaling and vascular development in mammals. Elife 2017;6.
[19] Klotz L, Norman S, Vieira JM, et al. Cardiac lymphatics are heterogeneous in origin and respond to injury. Nature 2015;522(7554):62–7.
[20] Lv C, Wu X, Wang X, et al. The gene expression profiles in response to 102 traditional Chinese medicine (TCM) components: a general template for research on TCMs. Sci Rep 2017;7(1):352.
[21] Urquhart J, Patterson RE, Bacharach SL, et al. Comparative effects of verapamil, diltiazem, and nifedipine on hemodynamics and left ventricular function during acute myocardial ischemia in dogs. Circulation 1984;69(2):382–90.
[22] West MB, Rokosh G, Obal D, et al. Cardiac myocyte-specific expression of inducible nitric oxide synthase protects against ischemia/reperfusion injury by preventing mitochondrial permeability transition. Circulation 2008;118(19):1970–8.
[23] Hoffmeyer MR, Jones SP, Ross CR, et al. Myocardial ischemia/reperfusion injury in NADPH oxidase-deficient mice. Circ Res 2000;87(9):812–7.
[24] Chen F, Li L, Tian DD. Salvia miltiorrhiza roots against cardiovascular disease: consideration of herb-drug interactions. Biomed Res Int 2017;2017 (9868694).
[25] Xu H, Li Y, Che X, Tian H, Fan H, Liu K. Metabolism of salvianolic acid A and antioxidant activities of its methylated metabolites. Drug Metab Dispos 2014;42(2):274–81.
[26] Han JY, Fan JY, Horie Y, et al. Ameliorating effects of compounds derived from Salvia miltiorrhiza root extract on microcirculatory disturbance and target organ injury by ischemia and reperfusion. Pharmacol Ther 2008;117(2):280–95.
[27] Cheng TO. Cardiovascular effects of Danshen. Int J Cardiol 2007;121(1):9–22.
[28] Fu Y, Liu HW, Forsythe SM, et al. Mutagenesis analysis of human SM22: characterization of actin binding. J Appl Physiol (1985) 2000;89(5):1985–90.
[29] Lin Y, Buckhaults PJ, Lee JR, et al. Association of the actin-binding protein transgelin with lymph node metastasis in human colorectal cancer. Neoplasia 2009;11(9):864–73.
[30] Uhlen M, Oksvold P, Fagerberg L, et al. Towards a knowledge-based human protein atlas. Nat Biotechnol 2010;28(12):1248–50.
[31] Goodman A, Goode BL, Matsudaira P, Fink GR. The Saccharomyces cerevisiae calponin/transgelin homolog Scp1 functions with fimbrin to regulate stability and organization of the actin cytoskeleton. Mol Biol Cell 2003;14(7):2617–29.
[32] Wamhoff BR, Hoofnagle MH, Burns A, Sinha S, McDonald OG, Owens GK. A G/C element mediates repression of the SM22alpha promoter within phenotypically modulated smooth muscle cells in experimental atherosclerosis. Circ Res 2004;95(10):981–8.
[33] Lagrand WK, Niessen HW, Wolbink GJ, et al. C-reactive protein colocalizes with complement in human hearts during acute myocardial infarction. Circulation 1997;95(1):97–103.
[34] Li Y, Feng J, Mo Y, Liu H, Yang B. Concordance between cardio-protective effect on isoproterenol-induced acute myocardial ischemia and phenolic content of different extracts of *Curcuma aromatica*. Pharm Biol 2016;54(12):3226–31.
[35] Senthil S, Chandramohan G, Pugalendi KV. Isomers (oleanolic and ursolic acids) differ in their protective effect against isoproterenol-induced myocardial ischemia in rats. Int J Cardiol 2007;119(1):131–3.
[36] Senthil S, Sridevi M, Pugalendi KV. Cardioprotective effect of oleanolic acid on isoproterenol-induced myocardial ischemia in rats. Toxicol Pathol 2007;35(3):418–23.
[37] Haleagrahara N, Varkkey J, Chakravarthi S. Cardioprotective effects of glycyrrhizic acid against isoproterenol-induced myocardial ischemia in rats. Int J Mol Sci 2011;12(10):7100–13.
[38] Zheng YY, Zhang HH, Yan XX, et al. Protective effect of low dose gadolinium chloride against isoproterenol-induced myocardial injury in rat. Apoptosis 2015;20(9):1164–75.
[39] Loegering DJ, Feintuch JJ, Carr FK. Reticuloendothelial system function following isoproterenol-induced myocardial injury. Am J Physiol 1979;236(6):H813–7.
[40] Liang Y, Liu D, Ochs T, et al. Endogenous sulfur dioxide protects against isoproterenol-induced myocardial injury and increases myocardial antioxidant capacity in rats. Lab Invest 2011;91(1):12–23.
[41] Giudice PL, Bonomini M, Arduini A. A moderate carnitine deficiency exacerbates isoproterenol-induced myocardial injury in rats. Cardiovasc Drugs Ther 2016;30(2):119–27.
[42] Panda VS, Naik SR. Cardioprotective activity of Ginkgo biloba phytosomes in isoproterenol-induced myocardial necrosis in rats: a biochemical and histoarchitectural evaluation. Exp Toxicol Pathol 2008;60(4–5):397–404.
[43] Rajadurai M, Stanely Mainzen Prince P. Preventive effect of naringin on cardiac markers, electrocardiographic patterns and lysosomal hydrolases in normal and isoproterenol-induced myocardial infarction in Wistar rats. Toxicology 2007;230(2–3):178–88.
[44] Vennila L, Pugalendi KV. Protective effect of sesamol against myocardial infarction caused by isoproterenol in Wistar rats. Redox Rep 2010;15(1):36–42.
[45] Mehdizadeh R, Parizadeh MR, Khooei AR, Mehri S, Hosseinzadeh H. Cardioprotective effect of saffron extract and safranal in isoproterenol-induced myocardial infarction in wistar rats. Iran J Basic Med Sci 2013;16(1):56–63.